CHEMISTRY
A EUROPEAN JOURNAL

DOI: 10.1002/chem.200701368

Liquid-Crystalline Rigid-Core Semiconductor Oligothiophenes: Influence of Molecular Structure on Phase Behaviour and Thin-Film Properties

Manuela Melucci,*[a] Laura Favaretto,[a] Christian Bettini,[a] Massimo Gazzano,[a] Nadia Camaioni,[a] Piera Maccagnani,[b] Paolo Ostoja,[b] Magda Monari,[c] and Giovanna Barbarella[a]

Abstract: The design, synthesis and properties of liquid-crystalline semiconducting oligothiophenes containing dithienothiophene (DTT), benzothiadiazole (BTZ) and carbazole (CBZ) rigid cores are described. The effect of molecular structure (shape, size and substitution) on their thermal behaviour and electrical properties has been investigated. Polarised optical microscopy (POM) and differential scanning calorimetry (DSC) analyses have revealed highly ordered smectic mesophases for most of the newly synthesised compounds. X-ray diffraction (XRD) studies performed at various temperatures have shown that the smectic order is retained in the crystalline state upon cooling across the transition temperature, affording cast films with a more favourable morphology for FET applications.

Keywords: liquid crystals · oligothiophenes · self-assembly · semiconductors · thin films

Introduction

Thiophene-based materials are of crucial interest in optoelectronics owing to their notable charge-transport and light-emission properties which are tuneable by a rational molecular design.[1]

Several classes of oligothiophenes have been proposed for applications in field-effect transistors (FET)[2] and the need for appropriate thin-film morphologies to achieve good device performance has been widely demonstrated.[3]

Oligothiophenes are usually crystalline materials and, in most cases, their cast films suffer from grain-boundary effects or crystallographic defects which are detrimental to charge transport. Very often, expensive techniques such as vacuum sublimation are required to obtain good quality thin films that satisfy the requirements for FETs. However, solution-processing[4] and, in general, low-cost deposition techniques are preferred for large-area application.

Recently, the ability of liquid-crystalline (LC) π-conjugated materials to give macroscopically ordered films with good charge-transport properties has been highlighted. Discotic, smectic and even nematic liquid crystals exhibit good carrier mobilities in their mesophases.[5–8] In particular, in smectic mesophases the short intermolecular distances of the mesogens within the mesophase layer confers a crystal-like molecular ordering over large continuous domains which favours the charge-carrier transport capability.

The interest in liquid crystals also lies in the possibility of freezing ordered LC states by cooling across the transition temperature. This thermal treatment often allows favourable morphologies to be achieved for FET applications.[9] Recently it was demonstrated that homeotropic alignment of a phenyl-thienyl co-oligomer in large monodomains can be achieved by simple melting of the cast film directly into the FET channel leading to a marked improvement in the electrical performance.[10]

One way to achieve LC properties in oligothiophenes is to add long aliphatic chains to one or both ends of unsubstituted rod-like oligomers.[11] By this approach the balance between the order induced by the aromatic rigid backbone and the disorder induced by the flexible alkyl ends usually

[a] Dr. M. Melucci, L. Favaretto, C. Bettini, Dr. M. Gazzano, Dr. N. Camaioni, G. Barbarella
Consiglio Nazionale Ricerche, CNR-ISOF
via P. Gobetti 101, I-40129 Bologna (Italy)
Fax: (+39) 5163-9834-9
E-mail: mmelucci@isof.cnr.it

[b] Dr. P. Maccagnani, Dr. P. Ostoja
Consiglio Nazionale Ricerche
Istituto di Microelettronica e Microsistemi
via P. Gobetti, 101, I-40129, Bologna (Italy)

[c] Prof. M. Monari
Dipartimento di Chimica 'G. Ciamician'
Università di Bologna, via Selmi 2, I-40126 Bologna (Italy)

Supporting information for this article is available on the WWW under http://www.chemeurj.org/ or from the author.

leads to LC behaviour that is strongly affected by the nature, size and position of the substituents.[9b,12] As an alternative, a "desymmetrisation" approach involving the design of asymmetric oligothiophenes that have two different alkyl ends[12b] has also been proposed to prevent the formation of polycrystalline films.

Up to now, only a few examples of bent-core molecules containing thiophene moieties in the aromatic backbone have been reported.[9b,13] Bent-core mesogens are the subject of great current interest because they can form mesophases with ferroelectric properties.[14]

In this work we have explored the thermal behaviour of a new class of thiophene molecular compounds that have rigid inner cores and flexible ends. By changing the nature of the rigid core unit, rod-like or bent oligomers were obtained. Dithienothiophene (DTT) and benzothiadiazole (BTZ) rigid cores were chosen to prepare rod-like oligomers and 9-methyl-9*H*-carbazole (CBZ) was selected to prepare bent-shaped cores.[15] Rigid cores, in particular carbazole ones, are known for their ability to enhance the thermal stability of organic molecules.[16] Moreover, strong π–π stacking in the crystal packing originated by these systems is expected to promote highly ordered smectic phases and consequently enhanced charge-transport capability.[17]

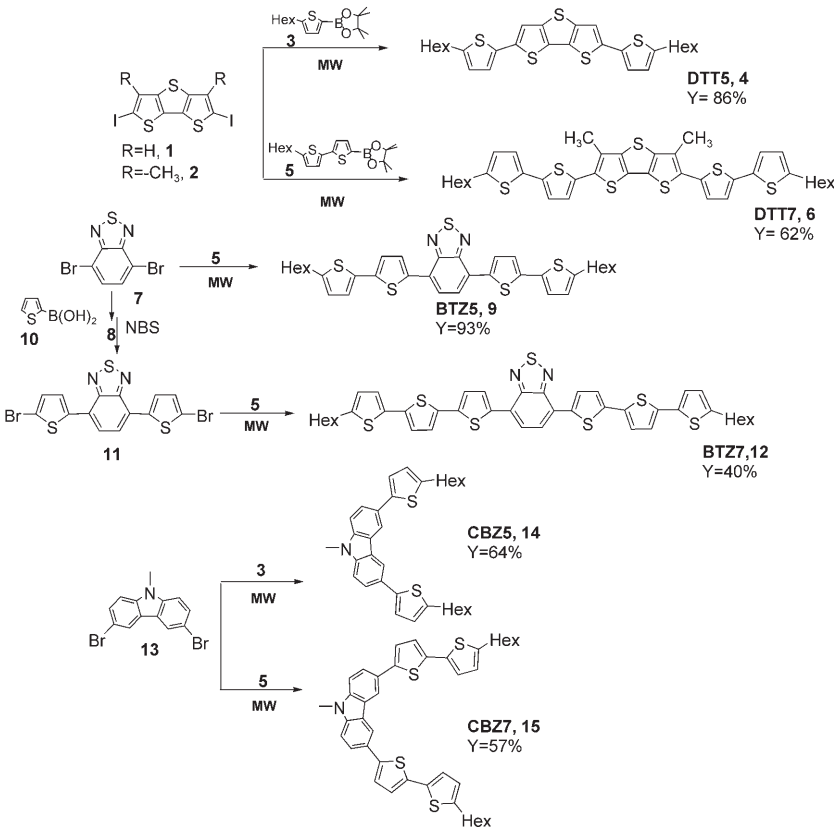

Scheme 1. Microwave-assisted synthesis of rigid-core oligothiophenes. Hex = *n*-hexyl.

Herein we report the efficient synthesis by microwave-assisted Suzuki coupling of oligothiophenes containing inner DTT, BTZ and CBZ cores and the study of the effect of their molecular structure (type of rigid core, length of the oligomer, relative size of the aromatic backbone and alkyl ends) on the thermal behaviour. The preliminary results of a study of their electrical properties are also given.

Results and Discussion

Molecular design and synthesis of rigid-core oligothiophenes: Scheme 1 shows the molecular structures of all the compounds prepared and the synthetic approach employed, namely, binding the central rigid core units to thienyl or bithienyl lateral groups. Initially, we prepared all the compounds by performing the Suzuki–Miyaura cross-coupling reaction[18] of dibromo or diiodo rigid cores, obtained with *N*-bromosuccinimide (NBS) or *N*-iodosuccinimide (NIS) by conventional procedures, and mono- or bithienylylpinacolatoborolane by using [$PdCl_2$(dppf)] (dppf = 1,1′-bis(diphenylphosphino)ferrocene) as the palladium source, KF as the base and DMF or DMSO (100 °C) as the solvent (Scheme 1). In this way, **BTZ5** (**9**) was obtained in 52 % yield after 6 h in refluxing DMF and **CBZ5** (**14**) and **CBZ7** (**15**) in 32 and 16 % yields, respectively, after 8 h and repeated addition of the palladium catalyst.

The long reaction times and the low yields achieved prompted us to explore the effect of microwave activation on the preparation of the oligomers. In agreement with what we had already observed for conventional oligothiophenes,[19] the yields were markedly improved (up to 90 %, Scheme 1) and the reaction times lowered from several hours to a few minutes.

All the syntheses were scaled up to the 0.5 g scale with isolated yields comparable and in some cases even better than those obtained on the 50 mg scale.

Compounds **4**, **6**, **9**, **14** and **15** were soluble in common organic solvents such as toluene, xylene, THF and chloroform with maximum attainable concentrations of about 5–10 mg mL^{-1}, the solubility decreasing on increasing the number of conjugated rings. **BTZ7** (**12**) needed slight heating (50–70 °C) for complete dissolution (max conc. 5 mg mL^{-1}).

Table 1. Transition temperatures and melting enthalpies for compounds **4**, **6**, **9**, **12**, **14** and **15**.[a]

Compound	Transition temperature [°C] (melting enthalpies [J g^{-1}])						
	Heating (20 °C min^{-1})				Cooling (20 °C min^{-1})		
DTT5 (**4**)	85 (3.8)	133 (6.7)	143 (45.0)	161 (0.7)	157 (1.3)	118–121 (50.0)	78 (2.6)
	K→K$_G$	K$_G$→SmB	SmB→N	N→I	I→N	N→Sm/K$_G$	K$_G$→K
DTT7 (**6**)	183 (43.0)	224 (1.5)	272 (1.03)		258 (0.7)	205 (18.2)	
BTZ5 (**9**)	136 (22.0)	178 (44.0)	205 (1.9)	213 (1.4)	206 (1.2)	164.5 (35.4)	
	K→SmX	SmX→SmG	SmG→N	N→I	I→SmG	SmX→K$_2$	
BTZ7 (**12**)	228 (22.8)				212 (19.7)		
CBZ5 (**14**)	143 (42.3)				131 (43.9)		
CBZ7 (**15**)	141 (14.0)	149 (21.9)			139 (26.0)	129 (1.25)	124 (12.1)

[a] K: crystalline, K$_G$: soft crystal phase,[20] Sm: smectic, SmX: undefined smectic, N: nematic, I: isotropic. DSC traces are given in the Supporting Information (Figure SI-1).

Thermal behaviour and phase characterisation by polarised microscopy, differential scanning calorimetry and X-ray diffraction: The thermal behaviour of compounds **4**, **6**, **9**, **12**, **14** and **15** was investigated by combining both hot-stage polarised microscopy (POM) and differential scanning calorimetry (DSC) analyses. Table 1 summarises the transition temperatures, the enthalpy values of the transitions of all the compounds and gives tentative phase assignments for compounds **4** and **9**.[20] It is seen that four of the six compounds examined display liquid-crystalline properties. The two compounds with the DTT rigid core, **4** and **6**, are liquid crystals. Of the BTZ core derivatives **9** and **12**, only the former, that is, the shortest one, displays LC behaviour. In contrast, for bent-shaped CBZ core derivatives, it is only the longest oligomer, **15**, that exhibits LC behaviour. Note that a lack of LC properties has been observed for other strongly angled compounds that have two, three or four aromatic rings.[14] Clearly, LC behaviour is a result of a balance of factors, from the type of rigid core to the relative size of the aromatic and aliphatic parts of the molecule, which makes it difficult to a priori predict those molecules that will exhibit LC properties. However, it seems that for rod-like systems it is the type of rigid core rather than the oligomer size that plays the main role in promoting LC properties. Moreover, as already observed for α,α′-didecyloligothiophenes of different length,[11a] the clearing point of rod-like oligomers increases with the number of conjugated rings.

Most liquid crystals tend to give polycrystalline films when cooled below their melting points. In this way they lose the molecular order that is characteristic of the liquid-crystalline mesophase with a consequent lowering of charge-transport ability. This is not the case for compounds **4** and **6** for which we were able, by the aid of X-ray diffraction investigations, to demonstrate that the high order characterising the smectic mesophases is retained in the solid state by cooling across the phase-transition temperature.

Exploring the LC properties, POM analysis of **DTT5** (**4**) shows heterogeneous nucleation occurs at 120 °C. Further heating to 135 °C leads to the appearance of fibril structures that grow anisotropically along one direction under isothermal conditions. The fibrils were highly birefringent, however, the phase was rather fluid excluding a crystalline phase. Further heating of the sample above 145 °C led to a bright, colourful and fluid Schlieren texture and finally isotropisation occurred at about 165 °C (Figure 1). On cooling the isotropic liquid of **DTT5** across the phase transition, droplets of Schlieren appeared at 154 °C which coalesced in a Schlieren domain observable over a very short range of temperatures (see Figure SI-2 in the Supporting Information).

A slight cooling of this texture resulted in the formation of lancet-like domains from the Schlieren domain which coalesce into larger laminar domains under isothermal conditions at 135 °C. Interestingly, the size of the laminar domains could be increased up to the millimetre scale by repeating the heating/cooling procedure between 135 and 140 °C (Figure 1d–f).

These large laminar domains showed uniform birefringence under polarised light which indicates homogeneous alignment. They persisted to room temperature making this compound a promising material for FET applications.[10]

The phase evolution of DTT5 was also monitored by XRD. Figure 2 shows the variation of the XRD profile on increasing the temperature from room temperature to 145 °C and then cooling back to room temperature (scan rate 5 °C min^{-1}). The profiles were recorded at different times to check whether the phase stability was maintained on cooling to room temperature from 135 °C, as indeed was the case. The frozen phase displayed a strong Bragg reflection at $2\theta = 6.3°$ (d spacing of 14 Å). Assuming that the length of the DTT5 molecule in a full extended conformation (also adopted in the crystal form, see Figure SI-3,4 in the Supporting Information) is about 30 Å, we suggest that the molecules are assembled as shown in Figure 2, that is, arranged in parallel rows that are shifted by half a molecule. Presumably the face-to-face π–π interactions between the thiophene rings of adjacent rows are the driving force for this type of organisation. The second most intense peak in the XRD pattern at $2\theta = 22.4°$ (d spacing 4 Å) is likely to be related to a suitable periodicity for orbital overlap between facing thiophene rings. No reflections were observed at 145 °C in accordance with the loss of order shown by the high transition enthalpy values (see Table 1).

With **DTT7** (**6**), which has a higher number of conjugated thienyl units than **DTT5**, POM showed only one LC shimmering, yellow and very mobile phase texture just below the clearing point at about 280 °C. However, the DSC trace

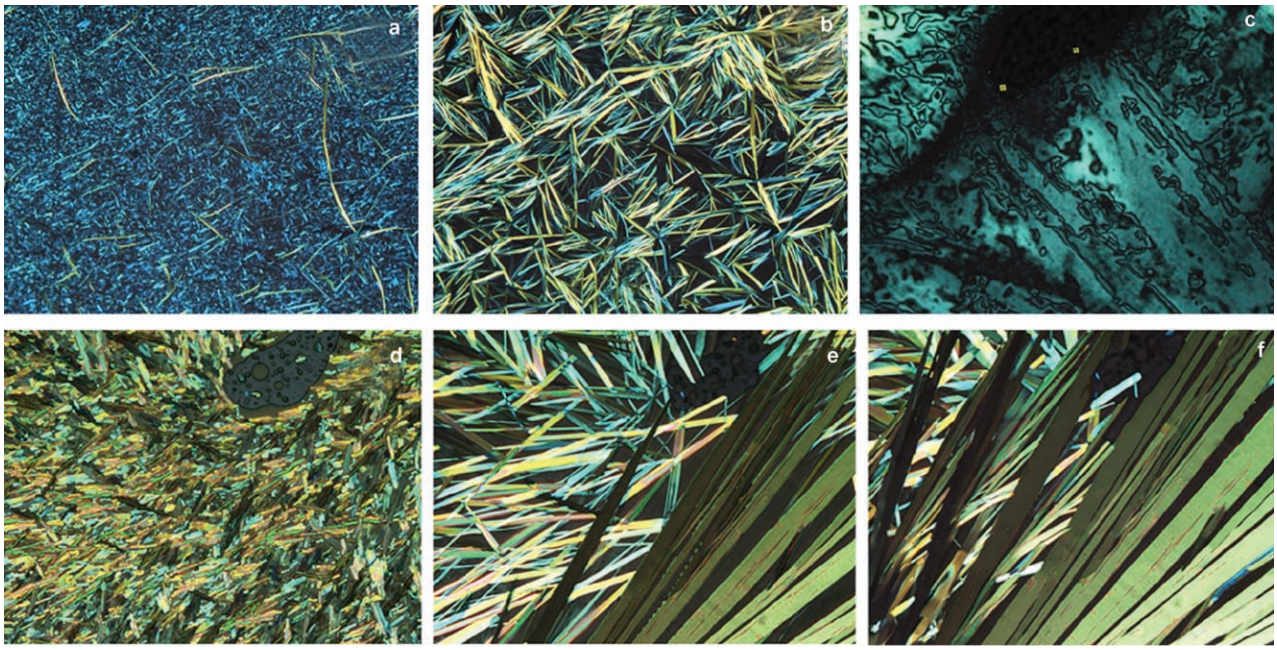

Figure 1. POM images of **DTT5** (**4**) showing the optical textures (crossed polars) of its phases (same region, from room temperature → 145 °C): a) fibril structures formed at 120 °C during the second heating; b) fibrils growth by keeping the temperature between 130 °C and 140 °C; c) Schlieren texture at 150 °C; (d, e, f) laminar domains growing from the melt by repeated melt-quench cycles 140 °C→135 °C→140 °C (first, second and third cycle, respectively). Image size 800μmx800μm.

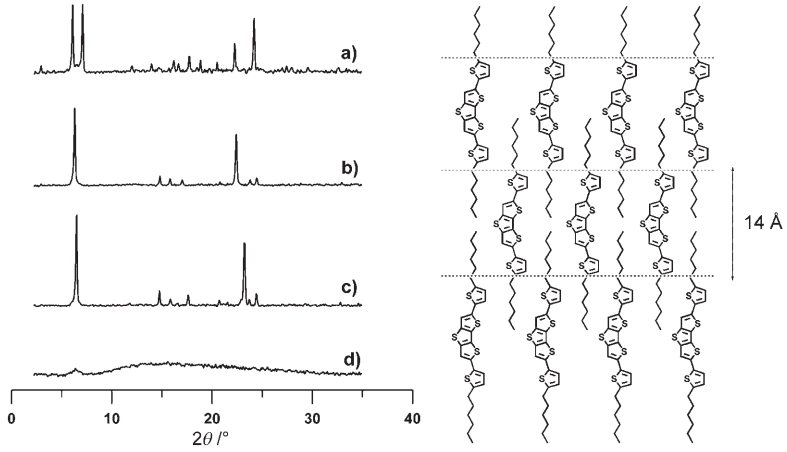

Figure 2. X-ray diffraction profiles of **DTT5** (**4**): a) at room temperature, b) at 130 °C on heating, c) at 70 °C upon cooling and d) at 145 °C on heating. The proposed organisation of **DTT5** molecules in the smectic mesophase is shown.

showed three transitions at 183, 224 and 272 °C, respectively (Table 1).

In contrast to **DTT7**, a good accord was found between the results obtained by DSC and POM for BTZ-core derivative **BTZ5** (**9**) which revealed four main phase transitions (Table 1). On heating to 140 °C a marked increase in birefringence and a higher fluidity were observed. Although phase identification was difficult, the relatively low enthalpy associated with that transition ($\Delta H = 22.3\ J\,g^{-1}$) indicates a highly ordered smectic phase (undefined Sm: SmX).

On further heating to 180 °C a mosaic texture appeared which turned into a birefringent fluid (reminiscent of a nematic texture)[20] at 200 °C ($\Delta H = 43.7\ J\,g^{-1}$). Finally, isotropisation occurred at 210 °C. On cooling the isotropic liquid viscous red droplets (similar to nematic droplets) appeared at 192 °C, which coalesced into a Sm mosaic texture (Figure 3c) at 185 °C. Crystallisation was not observed, however, thermal fractures (typical of the crystalline state) appeared at about 160 °C.

The variation of the XRD profile of **BTZ5** (**9**) on increasing the temperature from room temperature to the transition temperatures observed by DSC, that is, 80, 140 and 180 °C, is shown in Figure 3a.

The small-angle X-ray profile shows that the layer spacing is 25.3 Å at 80 °C (peak at $2\theta = 3.5°$), 29.2 Å (peak at $2\theta = 3.0°$) at 140 °C and 32.4 Å (peak at $2\theta = 2.7°$) at 180 °C (see Table SI-1 in the Supporting Information). The wide-angle diffraction shows several reflections that are multiple orders of the same *d* spacing which indicates the presence of a long-range positional order typical of a smectic structure.

As the extended molecular length of **BTZ5** is about 33 Å, the molecules must be arranged vertically to the substrate

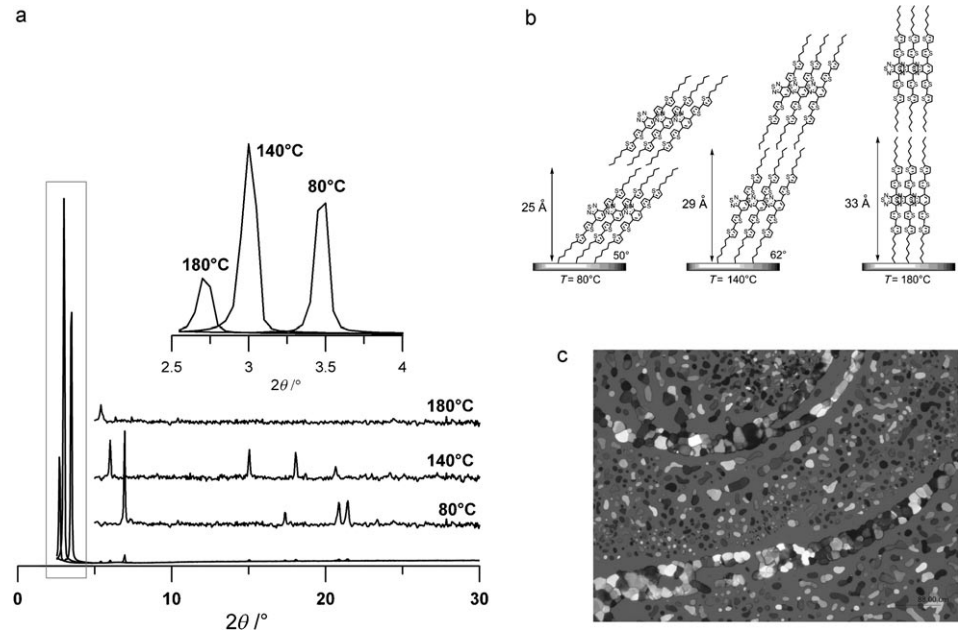

Figure 3. a) X-ray diffraction patterns of **BTZ5** recorded at 80, 140 and 180 °C. The small-angle region highlighted in the rectangle is expanded in the inset. b) The molecular arrangements of **BTZ5** (**9**) at 80, 140 and 180 °C. c) POM micrographs of a **BTZ5** film on untreated glass showing the mosaic texture at 180 °C.

with an inclination of 50° at 80 °C and 62° at 140 °C and be perpendicular to the glass surface at 180 °C (Figure 3b).

Interestingly, the POM and XRD analyses showed that the high order characterising the smectic phases of **BTZ5** could be easily frozen by cooling across the phase transition (rate 20 °C min^{-1}).

Figure 4a shows the XRD profile of the glassy phase quenched at 180 °C and that of the smectic phase at 180 °C. Although two phases are present, it is evident that most reflections at 180 °C are still present on quenching which means that the molecular arrangement at 180 °C is retained in the glassy phase.

The glassy films obtained by quenching the phases at 140 and 180 °C (glassy 140 and 180) showed a better coverage of the glass substrate (Figure 4b,c) than that cast at room temperature which makes **BTZ5** a promising substrate for FET applications.

Surprisingly, no evidence of liquid crystal phases was found for the longer BTZ core oligomer **12** which uniformly melted at 210 °C to give a viscous red fluid. DSC showed the melting peak at 228 °C ($\Delta H = 22.8$ J g^{-1}) and a reversible crystallisation at 212 °C ($\Delta H = 19.7$ J g^{-1}).

Concerning the bent CBZ derivatives, only the longest one, **CBZ7** (**15**), exhibited LC mesophases. Several textures within a narrow temperature range (rate 5 °C min^{-1}, Figure 5a) were observed. On cooling the isotropic liquid, three undefined textures consisting of brightly coloured areas, a shimmering texture and a mosaic texture were visible between 159 and 157 °C. On further cooling to 156 °C, dendritic nuclei were formed that coalesce to give the mosaic texture shown in Figure 5b (which points to a B1 mesophase[14]) which persisted to room temperature (thermal fractures could be observed within the domains). The mosaic consists of large isotropic domains with different optical activities. By rotating one polariser by a small angle from the crossed position, darker and brighter domains could be distinguished. By rotating in the opposite direction the dark area became birefringent and vice versa. Investigations into the electro-optical switching behaviour of this compound are currently under way.[21]

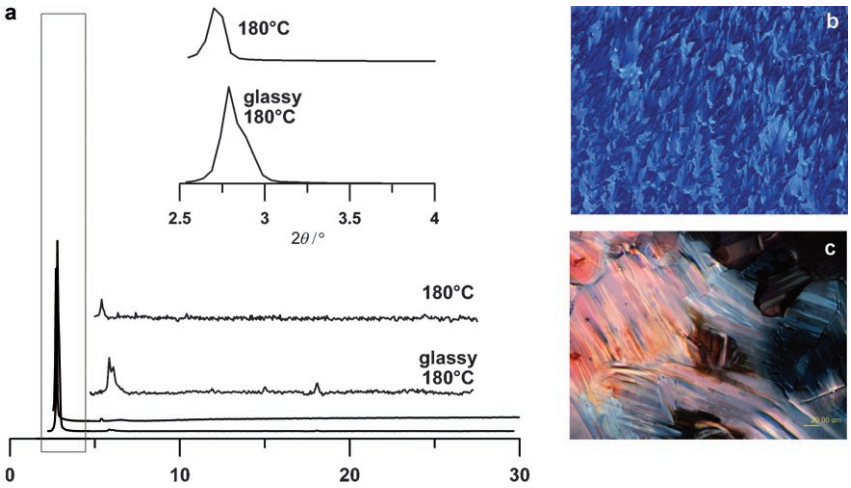

Figure 4. a) X-ray diffraction patterns of **BTZ5** (**9**) comparing the crystalline phase recorded at 180 °C with the phase obtained by freezing the mesophase at 180 °C (glassy 180 °C). The small-angle region highlighted in the rectangle is expanded in the inset. POM images of b) a **BTZ5** glassy SmX phase (cooling from 140 °C) and c) a glassy mosaic (cooling from 180 °C). Image size 800 μ × 800 μ.

Electrical characterisation: Owing to the high molecular order that characterises the solid films and their high solubility, all the compounds are potential candidates for the fabrication of efficient field-effect transistors (FETs) by solution-processing. Note that some of these materials show appreciа-

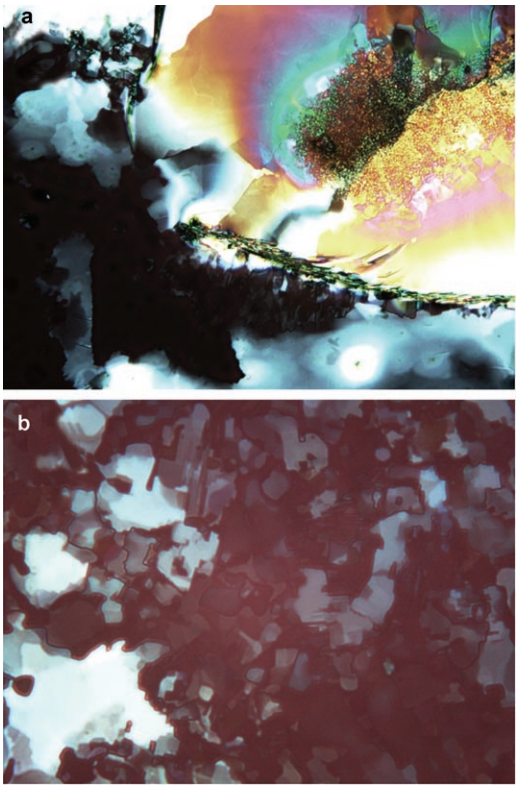

Figure 5. POM images (between crossed polarisers) of **CBZ7** (**15**): a) coexistence of different mesophases between 159 and 157 °C, b) the mosaic texture developed at 156 °C on cooling the isotropic melt. Images size (800 μm × 800 μm).

ble solid-state fluorescence emission which also makes them viable candidates for light-emitting field-effect transistors (LETs). Indeed, in a previous communication[22] we demonstrated the suitability of **DTT7** (**6**) as an active layer of a LET device. This compound has also been demonstrated to form bicolour fluorescent pixels by surface-tension-driven deposition.[23]

To evaluate their semiconducting properties, all the compounds were used as active layers in bottom-contact FETs. Moreover, owing to the ability of **DTT5** to form large domains upon annealing at about 135 °C and the possibility of freezing these ordered domains at room temperature (Figure 1), we also performed preliminary tests to compare the electrical conductivity of as-cast **DTT5** films with those of annealed samples. In this case, the electrical characterisation was carried out by using a two-electrode device under vacuum.

Characterisation in three-electrode devices (FET): Field-effect transistors that have both cast (from a toluene solution, 1 mg mL^{-1}) and vacuum-sublimed films films as active elements were prepared and tested at room temperature under an ambient atmosphere. The plots of the drain current I_D versus drain voltage V_D at different gate voltages V_G and that of I_D versus V_G are reported in the Supporting Information (Figure SI-5). Charge mobility values μ and $I_{on/off}$ current ratios were calculated by using the standard FET equations for a saturated regime and are listed in Table 2.

Table 2 shows that, in contrast to conventional oligothiophenes, which usually show much better charge-transport capability in vacuum-sublimed rather than solution-cast films, rigid-core oligothiophenes, independent of the type of rigid core and oligomer size, display charge-mobility values in cast films that are comparable to those of sublimed films. The data reported in Table 2 were obtained without device optimisation and it is likely that deposition performed under a more controlled environment or by using modern patterning techniques could lead to higher quality films and enhanced charge-mobility values.

We found that the film-forming properties of rigid-core oligothiophenes were markedly improved by cooling melted samples, obtained by simple solution casting, across the transition temperatures (glassy LC mesophase). Figure 6 compares the current–voltage *I–V* plots obtained for an as-cast film of **BTZ5** and for the same film obtained after heating at the transition temperatures and then cooling to room temperature. A marked increase in the current can be noted in the *I–V* plots in Figure 6 which is probably due to better homogeneity of the glassy films compared with the as-cast one. Moreover, an $I_{on/off}$ increase of up to three orders of magnitude was observed for the glassy films which is probably due to a better interface contact between the organic layer and the gold electrodes.

Table 2. Field-effect hole mobilities and on/off ratios for compounds **4**, **6**, **9**, **12**, **14** and **15** measured under ambient conditions without device optimisation.

Compound	Vacuum-evaporated films		Cast films	
	μ [cm^{2}V^{-1}s^{-1}]	$I_{on/off}$	μ [cm^{2}V^{-1}s^{-1}]	$I_{on/off}$
DTT5 (**4**)	1×10^{-5}	10^4	7×10^{-5}	10^3
DTT7 (**6**)[a]	2×10^{-2}	10^6	1×10^{-2}	10
BTZ5 (**9**)	2×10^{-4}	10^2	4×10^{-4}	10^3
BTZ5 (**9**) (glassy 140)[b]			2×10^{-4}	10^4
BTZ5 (**9**) (glassy 180)[c]			5×10^{-4}	10^6
BTZ7 (**12**)	2×10^{-4}	10^5	nd[d]	nd[d]
CBZ5 (**14**)[e]	–	–	–	–
CBZ7 (**15**)	7×10^{-5}	10^4	5×10^{-5}	10^5

[a] From ref. [22], measured under vacuum. [b] Obtained by cooling the sample from 140 °C to room temperature (~10 °C min^{-1}). [c] Obtained by cooling the sample from 180 °C to room temperature (~10 °C min^{-1}). [d] Data not available owing to the poor solubility of **BTZ7**. [e] No field-effect behaviour was observed for this compound.

Characterisation in two-electrode devices: Figure 7 shows the log–log current density–voltage (*J–V*) plots of an as-cast **DTT5** film and compares it with that obtained after anneal-

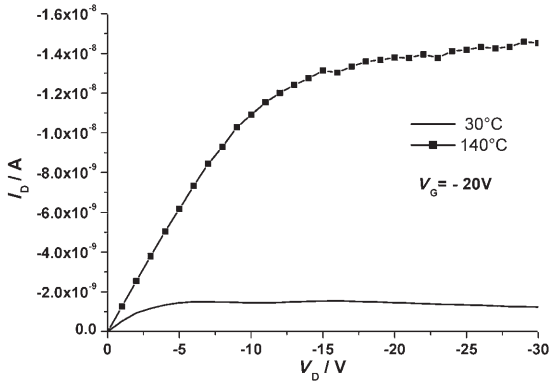

Figure 6. Current–voltage plots for a bottom-contact FET device based on a **BTZ5** film cast from toluene solution at room temperature as-cast (——) and by maintaining the substrate at the transition temperature of 140 °C and then cooling to room temperature (■, glassy 140). The measurements were carried out under ambient conditions.

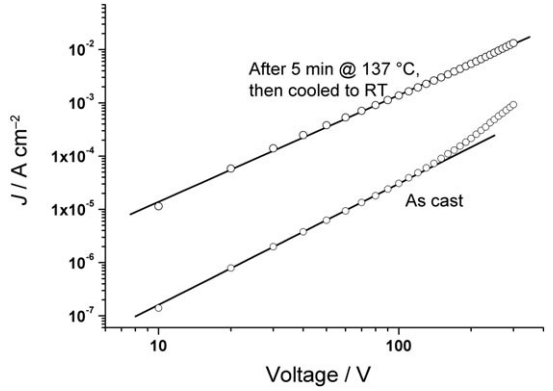

Figure 7. Room-temperature *J–V* curves for a **DTT5** film cast onto interdigitated gold electrodes: as-cast and after annealing at 137 °C for 5 minutes and then cooling to room temperature. The measurements were carried out under a dynamic vacuum of 10^{-5} mbar. The lines, with slope 2, represent linear fits to the experimental data.

ing the sample at 137 °C for 5 min and then cooling it to room temperature. Various annealing times were investigated and the current values were enhanced by increasing the time from 1 to 5 minutes. No further significant current variations were obtained for longer annealing times which suggests that the growing laminar crystalline domains, observed by POM microscopy (Figure 1f), reach a stable configuration after about 5 min annealing.

Figure 7 shows that there is an increase in current of about two orders of magnitude upon annealing the sample. Furthermore, in the investigated voltage range, the current density shows an excellent quadratic dependence on the voltage. This behaviour is typical of trap-free space-charge limited current (SCLC).[24]

A hole mobility of $3.7\times10^{-3}\,cm^2V^{-1}s^{-1}$ was estimated[25] for **DTT5** upon annealing. The estimated charge mobility for the as-cast film, about two orders of magnitude lower than that of the annealed film, is consistent with the measured field-effect mobility reported in Table 2 for **DTT5**.

Note that the mobility values for smectic liquid crystalline semiconductors can be optimised by improving the molecular alignment on the device surface. In particular, as already reported,[10,26] using silane-treated SiO_2/Si surfaces may help the homeotropic alignment of the molecules into a single monodomain. Detailed investigations of the FET behaviour of **DTT5** films upon annealing at the transition temperatures using silane-treated FET devices are currently under way.

Conclusion

Our results show that inserting an inner rigid core into the backbone of α-linked oligothiophenes terminated with hexyl chains is a successful strategy to promote liquid-crystalline behaviour. The LC behaviour depends on a balance of factors, including the nature of the rigid core and the molecular shape. The shorter oligomers, **DTT5** and **BTZ5**, exhibited several highly ordered mesophases, whereas a more limited number of phase transitions or no LC behaviour was observed for the longer oligomers. A better balance between the size of the aromatic backbone and the length of the aliphatic end-chains is probably needed to induce a more accentuated LC behaviour in the longer oligomers.

Our results also show that in the liquid-crystalline oligomers **DTT5** and **BTZ5**, the order that characterises the smectic mesophases can be retained by cooling to room temperature. In this way, ordered films with a morphology more suitable for charge transport can be obtained.

Preliminary electrical characterisations show such materials are promising as active layers in solution-processed field-effect transistors. Studies in this area are currently under way.

Experimental Section

General: Microwave-assisted reactions were carried out in air by using a Synthewave 402 (Prolabo) system with variable power and at a fixed temperature. Analytical thin-layer chromatography (TLC) was carried out by using 0.2 mm sheets of silica gel 60 F_{254} and visualisation was accomplished by using UV light (356 and 254 nm). Spectroscopic grade solvents (Aldrich) were used in the preparation of the solutions for film deposition.

A Nikon Eclipse 80i optical microscope was used for optical measurements. The images were recorded with a digital Nikon Coolpix 5400 colour camera. Glass substrates were furnished by Knittel Gläser and were washed with spectroscopic grade acetone (Aldrich) before use. Powder samples were sandwiched between two untreated glass plates and DSC traces were recorded under atmospheric conditions (see Figure SI-2 in the Supporting Information). No thermal degradation was observed for any of the samples after several heating/cooling cycles or by changing the scan rate.

XRD measurements were carried out at room temperature with a Bragg/Brentano diffractometer (X′pertPro Panalytical) equipped with a fast X′Celerator detector by using a copper anode as the X-ray source (Kα, $\lambda = 1.5418$ Å). Real-time XRD patterns at different temperatures were

collected by using an Anton Paar TTK450 heating attachment. Simulated X-ray diffraction patterns were obtained by using the PowderCell program.[27]

Single-crystal X-ray crystallography: X-ray diffraction intensities for DTT5 were collected on a Bruker SMART APEX II CCD diffractometer ($Mo_{K\alpha}$ radiation, $\lambda = 0.71073$ Å) at room temperature. Data were processed by using the Bruker SAINT package.[28] The structure was solved by direct methods (SIR97)[29] and refined on F^2 by using SHELXL-97[30] (see Figure SI-3 of the Supporting Information). Hydrogen atoms were calculated and refined as riding atoms. Crystal data for **DTT5**: formula $C_{28}H_{32}S_5$, $M_r = 528.84$, monoclinic, space group $P2_1/n$, $a = 14.919(7)$, $b = 5.653(3)$, $c = 32.732(16)$ Å, $\beta = 101.767(8)°$, $V = 2702(2)$ Å^3, $Z = 4$, $\rho_{calcd} = 1.300$ Mg m^{-3}, $\mu = 0.444$ mm^{-1}, $F(000) = 1120$, $T = 296(2)$ K, $\theta_{max} = 25.41$, 18830 reflections collected, 2168 with $I > 2(\sigma(I))$. Final $R_1 = 0.1188$, $wR_2 = 0.2862$, GOF = 1.679.

CCDC-655866 contains the supplementary crystallographic data for this paper. These data can be obtained free of charge via www.ccdc.cam.ac.uk/data_request/cif

FET fabrication: Heavily doped <100> n-Si wafers were used as substrates and a layer of 150 nm of SiO_2 (grown by thermal oxidation) was used as the gate dielectric. Gold (80 nm) was evaporated and photolithographically defined to obtain the electrodes for the gate, source and drain. The source and drain electrodes had a circular structure with a channel width of 1880 μm and a channel length of 40 μm. Thin films were prepared by thermal evaporation onto substrates held at a constant temperature or by casting on top of the substrates. The electrical measurements were recorded by using a computer-controlled parametric characterisation system at room temperature under atmospheric pressure.

Two-electrode device fabrication: The substrates consisted of two interdigitated gold electrodes (the spacing between the two electrodes was 20 μm) deposited onto a layer of silicon dioxide (thickness = 1 μm) thermally grown on silicon plates. The active area, calculated from the free space between the gold fingers, was 4.35×10^{-4} cm^2. A planar geometry was chosen to avoid the common problem of evaporated gold electrodes on vertically structured samples, that is, its diffusion through the organic layer. The devices prepared were hole-only devices as gold acts as a hole-injecting contact. Indeed, the gold work function (5.2 eV) was energetically matched to the highest occupied molecular orbital energy levels of thiophene oligomers and prevented electron injection from the negatively biased electrode. **DTT5** films were cast from dichloromethane solution in order to completely cover the interdigitated area. The concentration of the solution was 20 g L^{-1} which led to films with a thickness (1.1–1.4 μm) greater than that of the electrode layer. The electrical characterisation was performed at room temperature (21 °C) under a dynamic vacuum (2×10^{-5} mbar). The current–voltage curves were recorded with a Keithley 487 source picoammeter.

Materials: Boronic esters **3** and **5** and 2,1,3-benzothiadiazole (BTZ) were purchased from Aldrich and used without further purification. The synthesis and characterisation of 2,6-bis-(5′-hexyl-2,2′-bithienyl-5-yl)-3,5-dimethyldithieno[3,2-*b*:2′,3′-*d*]thiophene (**DTT7**, **6**),[22] 4,7-dibromo-2,1,3-benzothiadiazole (**7**),[31] 4,7-bis(2-thienyl)-2,1,3-benzothiadiazole (**8**)[32] and 4,7-bis(5-bromo-2-thienyl)-2,1,3-benzothiadiazole (**11**)[33] have already been described. Dithieno[3,2-*b*:2′,3′-*d*]thiophene (DTT) and 9-methyl-9*H*-carbazole (CBZ) rigid cores were prepared by following previously described synthetic procedures.[34a,b]

2,6-Bis(5-hexyl-2-thienyl)dithieno[3,2-*b*:2′,3′-*d*]thiophene (DTT5, 4): A microwave oven reactor was charged with compounds **1** (0.114 g, 0.00026 mol) and **3** (0.3 g, 0.001 mol), KF (0.12 g, 0.0020 mol) and [$PdCl_2$(dppf)] as catalyst (5 mol %, 0.00932 g) dissolved in DMF (5 mL). The reagents were irradiated with microwaves at 100 °C for 20 min and then the solvent was evaporated under vacuum. The crude thus obtained was washed with H_2O and extracted with CH_2Cl_2. The organic phases were collected and dried over Na_2SO_4. After evaporation of the solvent, the crude was filtered trough an alumina cup with CH_2Cl_2 as the eluent. After crystallisation from toluene, **DTT5** was obtained as a yellow powder (0.118 g) in 86 % yield. M.p. 136 °C; ^{1}H NMR ($CDCl_3$, TMS): $\delta = 7.22$ (s, 2H), 7.00 (d, $J = 3.6$ Hz, 2H), 6.68 (m, 2H), 2.8 (t, 4H), 1.69 (m, 4H), 1.33 (m, 12H), 0.9 ppm (t, 6H); ^{13}C NMR ($CDCl_3$, TMS): $\delta = 145.9$, 141.2, 138.5, 134.8, 129.1, 123.6, 116.1, 31.6, 31.5, 30.5, 28.8, 22.7, 14.1 ppm; UV/Vis (CH_2Cl_2): $\lambda_{max} = 397$ nm; MS (70 eV, EI): *m*/*z*: 528 [$M^{\cdot+}$]; elemental analysis calcd (%) for $C_{28}H_{32}S_5$ (528.88): C 63.59, H 6.10; found: C 63.63, H 6.15.

4,7-Bis(5′-hexyl-2,2′-bithienyl-5-yl)-2,1,3-benzothiadiazole (BTZ5, 9): A microwave oven reactor was charged with compounds **7** (0.05 g, 0.00017 mol), **5** (0.159 g, 0.000425 mol), KF (0.157 g, 0.00272 mol) and [$PdCl_2$(dppf)] as catalyst (5 mol %, 0.007 g) dissolved in DMSO (5 mL). The reagents were irradiated with microwaves for 40 min at 100 °C. Then H_2O (10 mL) was added to the crude solution and the suspension centrifuged. The precipitate thus obtained was washed twice with H_2O then extracted with CH_2Cl_2. The organic phases were collected and dried over Na_2SO_4. After evaporation of the solvent, crystallisation from toluene/pentane afforded 9 (0.100 g) as a deep red powder (93 % yield). M.p. 156 °C; ^{1}H NMR ($CDCl_3$, TMS): $\delta = 8.03$ (d, $J = 4$ Hz, 2H), 7.83 (s, 2H), 7.19 (d, $J = 4$ Hz, 2H), 7.11 (d, $J = 3.2$ Hz, 2H), 6.72 (d, $J = 3.2$ Hz, 2H), 2.82 (m, 4H), 1.65 (m, 4H), 1.43 (m, 12H), 0.90 ppm (m, 6H); ^{13}C NMR ($CDCl_3$, TMS): $\delta = 152.7$, 146.1, 139.5, 137.6, 134.8, 128.4, 125.7, 125.2, 125.0, 123.9, 123.8, 31.6, 31.5, 30.3, 28.8, 22.6, 14.0 ppm; UV/Vis (CH_2Cl_2): $\lambda_{max} = 512$ nm; MS (70 eV, EI): *m*/*z*: 632 [$M^{\cdot+}$]; elemental analysis calcd (%) for $C_{34}H_{36}N_2S_5$ (632.99): C 64.51, H 5.73, N 4.43; found: C 64.58, H 5.69, N 4.42.

4,7-Bis(5″-hexyl-2:2′,5′:2″-terthienyl-5-yl)-2,1,3-benzothiadiazole (BTZ7, 12): Compound **11** (0.096 g, 0.0002 mol), **5** (0.188 g, 0.0005 mol), KF (0.186 g, 0.0032 mol) and [$PdCl_2$(dppf)] as catalyst (5 mol %, 0.0082 g) were introduced into the microwave oven reactor and dissolved in DMSO (6 mL). After irradiation at 100 °C for 40 min, H_2O (3 mL) was added to the crude solution and the resulting suspension centrifuged. The precipitate thus obtained was dissolved in warm toluene and filtered through silica gel with warm toluene as the eluent. The solution was evaporated and the product crystallised from toluene. Compound 12 was isolated in 40 % yield (0.064 g) as a dark brown powder. M.p. 202 °C; ^{1}H NMR ($CDCl_3 + CS_2$, TMS): $\delta = 8.07$ (d, $J = 4$ Hz, 2H), 7.85 (s, 2H), 7.22 (d, $J = 3.6$ Hz, 2H), 7.15 (d, $J = 3.6$ Hz, 2H),?7.01 (d, $J = 3.6$ Hz, 2H), 6.98 (d, $J = 4$ Hz, 2H), 6.68 (d, $J = 3.6$ Hz, 2H) 2.82 (m, 4H), 1.71 (m, 4H), 1.40 (m, 12H), 0.93 ppm (m, 6H); UV/Vis (CH_2Cl_2): $\lambda_{max} = 533$ nm; MS (70 eV, EI): *m*/*z*: 796 [$M^{\cdot+}$]; elemental analysis calcd (%) for $C_{42}H_{40}N_2S_7$ (797.24): C 63.27, H 5.06, N 3.51; found: C 63.20, H 5.10, N 3.52.

3,6-Bis(5-hexyl-2-thienyl)-9-methyl-9*H*-carbazole (CBZ5, 14): Compound **13** (0.160 g, 0.00047 mol), **3** (0.415 g, 0.00141 mol), KF (0.273 g, 0.0047 mol) and [$PdCl_2$(dppf)] as catalyst (5 mol %, 0.0019 g) were introduced into the microwave oven reactor and dissolved in DMF (12 mL). After MW irradiation at 100 °C for 40 min the solvent was evaporated and the crude washed with water and extracted with CH_2Cl_2. The organic phases were collected and dried over Na_2SO_4. Flash chromatography on silica gel with pentane/AcOEt (9:1) as eluent afforded compound 14 (0.154 g) in 64 % yield. M.p. 132 °C; ^{1}H NMR ($CDCl_3$, TMS): $\delta = 8.27$ (d, $J = 1.2$ Hz, 2H), 7.70 (dd, $J = 1.6$, 8.4 Hz, 2H), 7.35 (d, $J = 8.4$ Hz, 2H), 7.16 (d, $J = 3.6$ Hz, 2H), 6.77 (br d, $J = 3.6$ Hz, 2H), 3.85 (s, 3H), 2.85 (t, 4H), 1.65 (m, 4H), 1.43 (m, 12H), 0.91 ppm (m, 6H); ^{13}C NMR ($CDCl_3$, TMS): $\delta = 144.5$, 142.9, 140.7, 126.4, 125.0, 124.2, 123.2, 121.6, 117.5, 108.8, 31.7, 31.6, 30.3, 28.8, 27.7, 22.6, 14.1 ppm; UV/Vis (CH_2Cl_2): $\lambda_{max} = 323$ nm; MS (70 eV, EI): *m*/*z*: 513 [$M^{\cdot+}$]; elemental analysis calcd (%) for $C_{33}H_{39}NS_2$ (513.8): C 77.14, H 7.65, N 2.73; found: C 77.09, H 7.70, N 2.74.

3,6-Bis(5′-hexyl-2,2′-bithienyl-5-yl)-9-methyl-9*H*-carbazole (CBZ7, 15): A microwave oven reactor was charged with compound **13** (0.278 g, 0.0007 mol), **5** (0.786 g, 0.0021 mol), KF (0.65 g, 0.011 mol) and [$PdCl_2$-(dppf)] as catalyst (6 mol %, 0.034 g) dissolved in DMF (20 mL). The reagents were irradiated with microwaves for 50 min at 100 °C. The solvent was evaporated and the crude washed with water and extracted with CH_2Cl_2. The organic phases were collected and dried over Na_2SO_4. After evaporation of the solvent, crystallisation from toluene afforded 9 (0.270 g) as a deep-red powder (57 % yield). M.p. 137 °C; ^{1}H NMR ($CDCl_3$, TMS): $\delta = 8.31$ (br d, $J = 1.6$ Hz, 2H), 7.73 (d, $J = 1.6$ Hz, 2H), 7.36 (d, $J = 8.4$ Hz, 2H), 7.25 (d, $J = 3.6$ Hz, 2H), 7.10 (d, $J = 3.6$ Hz, 2H), 7.03 (d, $J = 3.6$ Hz, 2H), 6.71 (br d, $J = 3.6$ Hz, 2H), 3.84 (s, 3H), 2.82 (t,

4H), 1.7 (m, 4H), 1.38 (m, 12H), 0.91 ppm (m, 6H); ^{13}C NMR ($CDCl_3$, TMS): $\delta = 145.1$, 143.7, 141.0, 136.1, 135.1, 125.8, 124.7, 124.2, 123.9, 123.1, 122.9, 122.5, 117.5, 109.0, 31.6, 30.2, 29.3, 22.6, 14.1 ppm; UV/Vis (CH_2Cl_2): $\lambda_{max} = 372$ nm; MS (70 eV, EI): m/z: 677 [$M^{\bullet+}$]; elemental analysis calcd (%) for $C_{41}H_{43}NS_4$ (678.05): C 72.63, H 6.39, 2.07; found: C 72.68, H 6.33, N 2.06.

Acknowledgements

This work was partially supported by the projects "Nanoscale Integrated processing of self-organising Multifunctional Organic materials" (EU Integrated Project NAIMO, No. NMP4-CT-2004-500355) and FIRB RBNE03S7XZ_005 "SYNthEsis of novel oRGanic materials and supramolecular architectures for high efficiencY optoelectronic and photonic systems" (SYNERGY).

[1] G. Barbarella, M. Melucci, G. Sotgiu, *Adv. Mater.* **2005**, *17*, 1581–1593.
[2] a) S. A. Ponomarenko, E. A. Tatarinova, A. M. Muzafarov, S. Kirchmeyer, L. Brassat, A. Mourran, M. Moeller, S. Setayesh, D. de Leeuw, *Chem. Mater.* **2006**, *18*, 4101–4108; b) S. A. Ponomarenko, S. Kirchmeyer, A. Elschner, N. M. Alpatova, M. Halik, H. Klauk, U. Zschieschang, G. Schmid, *Chem. Mater.* **2006**, *18*, 579–586; c) M. Halik, H. Klauk, U. Zschieschang, G. Schimd, S. Ponomarenko, S. Kirchmeyer, W. Weber, *Adv. Mater.* **2003**, *15*, 917–922; d) A. R. Murphy, J. M. J. Fréchet, *Chem. Rev.* **2007**, *107*, 1066–1096.
[3] a) C. D. Dimitrakopoulos, P. R. L. Malenfant, *Adv. Mater.* **2002**, *14*, 99–117; b) J. Locklin, M. E. Roberts, S. C. B. Mannsfeld, Z. Bao, *J. Macromol. Sci., Part C: Pol. Rev.* **2006**, 79–101.
[4] H. Sirringhaus, *Adv. Mater.* **2005**, *17*, 2411–2425.
[5] a) D. Adam, P. Schuhmacher, J. Simmerer, L. Häussling, K. Siemensmeyer, K. H. Etzbach, H. Ringsdorf, D. Haarer, *Nature* **1994**, *371*, 141–143; b) A. M. van de Craats, J. M. Warman, A. Fechtenkotter, J. D. Brand, M. A. Harbison, K. Mullen, *Adv. Mater.* **1999**, *11*, 1469–1472; c) M. Funahashi, J. Hanna, *Mol. Cryst. Liq. Cryst.* **2004**, 410, 529–540; d) A. M. van der Craats, J. M. Warman, K. Mullen, Y. Geerts , J. D. Brand *Adv. Mater.* **1998**, 10, 36–38.
[6] H. Maeda, M. Funahashi, J. Hanna, *Mol. Cryst. Liq. Cryst.* **2001**, *366*, 369–376.
[7] M. Funahashi, J. Hanna, *Appl. Phys. Lett.* **2000**, *76*, 2574–2576.
[8] M. Funahashi, J. I. Hanna, *Adv. Mater.* **2005**, *17*, 594–598.
[9] a) K. L. Woon, M. P. Aldred, P. Vlachos, G. H. Mehl, T. Stirner, S. M. Kelly, M. O'Neill, *Chem. Mater.* **2006**, *18*, 2311–2317; b) A. J. J. M. Van Breemen, P. T. Herwig, C. H. T. Chlon, J. Sweelssen, H. F. M. Schoo, S. Setayesh, W. M. Hardeman, C. A. Martin, D. M. de Leeuw, J. J. P. Valeton, C. W. Bastiaansen, D. J. Broer, A. R. Popa-Merticaru, S. C. J. Meskers, *J. Am. Chem. Soc.* **2006**, *128*, 2336–2345.
[10] J. C. Maunoury, J. R. Howse, M. L. Turner, *Adv. Mater.* **2007**, *19*, 805–809.
[11] a) S. Ponomarenko, S. Kirchmeyer, *J. Mater. Chem.* **2003**, *13*, 197–202; b) F. Garnier, R. Haljlaoui, A. E. Kassmi, G. Horowitz, L. Laigre, W. Porzio, M. Armanini, F. Provasoli, *Chem. Mater.* **1998**, *10*, 3334–3339.
[12] a) H. Zhang, S. Shiino, A. Shishido, A. Kanazawa, O. Tsutsumi, T. Shiono, T. Ikeda, *Adv. Mater.* **2000**, *12*, 1336–1339; b) M. Funahashi, J. I. Hanna, *Adv. Mater.* **2005**, *17*, 594–598.
[13] a) Y. S. Park, D. Kim, H. Lee, B. Moon, *Org. Lett.* **2006**, *8*, 4699–4702; b) K. Kishikawa, M. C. Harris, T. M. Swager, *Chem. Mater.* **1999**, *11*, 867–871.
[14] a) G. Pelzl, S. Diele, W. Weissflog, *J. Adv. Mater.* **1999**, *11*, 707–725; b) W. L. MacMillan, *Phys. Rev. A* **1971**, *4*, 1238–1246; c) K. Kishikawa, M. C. Harris, T. M. Swager, *Chem. Mater.* **1999**, *11*, 867–871; d) T. Niori, T. Semine, J. Watanabe, T. Furukawa, H. Takezoe, *J. Mater. Chem.* **1996**, *6*, 1231–1233; e) D. R. Link, G. Natale, R. Shao, J. E. Maclennan, N. A. Clark, E. Korblova, D. M. Walba, *Science* **1997**, *278*, 1924–1927.
[15] M. Belloni, M. Manickam, P. Ashton, B. M. Kariuki, J. A. Preece, N. Spencer, J. Wilkie, *Mol. Cryst. Liq. Cryst.* **2001**, 369, 17–35.
[16] a) F. C. Yu, L. J. Yu, *Chem. Mater.* **2006**, *18*, 5410–5420; b) V. Promarak, S. Ruchirawar *Tetrahedron* **2007**, *63*, 1602–1609; c) B. E. Koene, D. E. Loy, M. E. Thompson, *Chem. Mater.* **1998**, *10*, 2235–2250.
[17] a) X. Zhang, J. P. Johnson, J. W. Kampf, A. J. Matzger *Chem. Mater.* **2006**, *18*, 3470–3476; b) R. D. Champio, K. F. Cheng, C. L. Pai, W. C. Chen, S. A. Jenekhe, *Macromol. Rapid Commun.* **1971**, *8*, 379–384.
[18] A. Suzuki *J. Organomet. Chem.* **1999**, *576*, 147–168.
[19] M. Melucci, G. Barbarella, M. Zambianchi, P. Di Pietro, A. Bongini, *J. Org. Chem.* **2004**, *69*, 4821–4824.
[20] I. Dierking, *Textures of Liquid Crystals*, Wiley-VCH, Weinheim, **2003**.
[21] a) F. C. Yu, L. J. Yu, *Chem. Mater.* **2006**, *18*, 5410–5420; b) W. Weissflog, U. Dunemann, M. W. Schröder, S. Diele, G. Pelzl, H. Kresse, S. Grande, *J. Mater. Chem.* **2005**, *15*, 939–946.
[22] F. Cicoira, C. Santato, M. Melucci, L. Favaretto, M. Gazzano, M. Muccini, G. Barbarella, *Adv. Mater.* **2006**, *18*, 169–174.
[23] I. Viola, F. Della Sala, M. Piacenza, L. Favaretto, M. Gazzano, M. Anni, G. Barbarella, R. Cingolani, G. Gigli, *Adv. Mater.* **2007**, *19*, 1597–1602.
[24] M. A. Lampert, P. Mark, *Current Injection in Solids*, Academic Press, New York, **1970**.
[25] Trap-free space-charge limited current is given by $j = {}^9/_8 \varepsilon_o \varepsilon_r \mu V^2 L^{-3}$, where ε_0 is the vacuum permittivity, ε_r is the relative dielectric constant of the material, μ is the charge-carrier mobility and L is the distance between the electrodes (20 μm in the present case). Although the trap-free limit is not experimentally accessible, the above formula can be used to extract a lower limit for the intrinsic mobility of the material (by using $\varepsilon_r = 3$), at least in the case in which one type of carriers (holes in this case) is responsible for charge transport (see ref. [24]).
[26] I. McCulloch, W. Zhang, M. Heeney, C. Bailey, M. Giles, D. Graham, M. Shkunov, D. Sparrowe, S. Tierney, *J. Mater. Chem.* **2003**, *13*, 2436–2444.
[27] PowderCell for Windows, version 2.3, W. Kraus, G. Nolze, Federal Institute for Material Research and Testing, Berlin, version 2.3, **1999**.
[28] SAINT frame integration software, Version 6.02a, BrukerXS, Inc, Madison, WI, **2000**.
[29] A. Altomare, M. Burla, M. Camalli, G. Cascarano, C. Giacovazzo, A. Guagliardi, A. Moliterni, G. Polidori, R. Spagna, *J. Appl. Crystallogr.* **1999**, *32*, 115–119.
[30] SHELXL-97, Program for Crystal Structure Solution, G. M. Sheldrick, University of Göttingen, Göttingen (Germany), **1997**.
[31] E. Bundgaard, F. C. Krebs, *Macromolecules* **2006**, *39*, 2823–2831.
[32] H. A. M. van Mullekom, J. A. J. M. Vekemans, E. W. Meijer, *Chem. Eur. J.* **1998**, *4*, 1235–1243.
[33] Q. Hou, Y. Xu, W. Yang, M. Yuan, J. Peng, Y. Cao, *J. Mater. Chem.* **2002**, *12*, 2887–2892.
[34] a) F. Allared, J. Hellberg, T. Remonen, *Tetrahedron Lett.* **2002**, *43*, 1553–1554; b) J. Bergman, P.-O. Norrby, P. Sand, *Tetrahedron* **1990**, *46*, 6113–6124.

Received: August 30, 2007
Revised: October 17, 2007
Published online: November 14, 2007

